

EPAIA: Design, modelling and control of a novel electro-pneumatic adaptable impedance actuator

Berno J.E. Misgeld, Joergen Stille, Anake Pomprapa, Steffen Leonhardt

*Chair for Medical Information Technology, Helmholtz-Institute for
Biomedical Engineering,
RWTH Aachen University, Aachen, Germany
(e-mail: misgeld@hia.rwth-aachen.de).*

Abstract: In this contribution we present the novel electro-pneumatic adaptable impedance actuator (EPAIA) consisting of a brushless DC-motor and a rotational pneumatic actuator, applied in series to the gear train. The pneumatic actuator is employed as a pneumatic torsional spring with a continuously adaptable stiffness, controlled by air inflow and pressure control. Thus, a rotary variable stiffness actuator is obtained, for which the stiffness can be expressed as a smooth nonlinear function of chamber pressures. The mechanical design furthermore utilises a planetary and a bevel gear reduction, to provide a torque amplification ratio necessary for human assistive knee joint actuation. Besides large and precise torque generation, the actuator provides a smoothly adjustable output impedance, backdrivability and a low cost, yet quality sensitive torque sensor. Following a detailed description of the mechanical design of the actuator, a dynamical model is derived using the Lagrange formalism. We propose a robust \mathcal{H}_2 -torque-controller design procedure for the linearised actuator model, for which a constraint for passivity of the load transfer function is employed. The resulting controller is tested in simulations using the nonlinear validated model.

Keywords: rehabilitation robotics, Euler-Lagrange modelling, electro-mechanical, pneumatic, control

1. INTRODUCTION

Human and animal locomotion has to be stable in face of an uncertain environment undergoing unknown disturbances. The human and animal musculo-skeletal system is thus well equipped with the ability to modulate mechanical impedance by antagonistic co-activation of muscles and nonlinear sinews, attached to the joint. The mechanical impedance, in this context, is the static and dynamic relationship between muscle-tendon complex (MTC) and velocity due to imposed stretch. Its important role in general locomotion and interaction with variable environments was investigated in the 1980's (Hogan (1984)) and still is an active research topic. Early investigations on muscular impedance working on a joint during human locomotion was for example reported by Cavagna et al. (1977). In addition to the compliant behaviour, necessary when interacting with the environment, the MTC is able to store and release energy in cyclic or explosive movements (Misgeld et al. (2012)). These properties are highly desirable in rehabilitation robotics applications, where actuator and trajectory control has to guarantee stable interaction with variable degree of support or compliant behaviour of the robotic manipulator.

Force or torque generating industrial manipulators are classically designed as highly stiff systems and are suited for tasks like high bandwidth positioning involving limited contact to the environment. In contrast to that, a new form of actuators that comprise an additional compliant element was introduced in the 1990's (Pratt and Williamson (1995); Pratt et al. (1995)). First applied to hydraulic and electric actuators, the use of an elastic element (spring), in series with actuator and load, was motivated by a number of reasons. Among the most prominent reasons to use a compliant element in an otherwise stiff actuator

is safety, which includes a stable human robot interaction and the minimisation of high energies due to end-effector collisions, Zinn et al. (2003). Other reasons are for example the energy storage in cyclic and explosive movements (Greibenstein et al. (2011)) and a cheap torque sensor, assuming the stiffness of the compliant element is known and the length or rotation angle difference of the spring can be measured. Compliant actuators have found their way into many application areas, like for example walking robots, robots that consider safe human-robot interaction and exoskeletons for rehabilitation and movement augmentation. Different compliant actuators have been introduced in the last two decades, but one of the main drawbacks, besides the additional mechanical element, is the limited bandwidth imposed by a fixed elastic element. This limitation is partially lifted by an active impedance control (or virtual stiffness control), where a virtual stiffness is set by a controller, that is closed around the impedance control-loop. However, the stiffness value cannot be increased above the stiffness value of the compliant element, without providing energy to the compliant element (Vallery et al. (2007)). Therefore, most recent approaches consider offline or online adjustable compliant elements (Ham et al. (2009)). However, drawbacks are the need for a second actuator and an often complicated mechanical set-up leading to heavy designs. Depending on the technology used, the compliant element may not be continuously adaptable under varying load conditions and may show adverse effects like backlash and hysteresis.

In this contribution, and in contrast to previous approaches, we present the design of a new continuously adjustable stiffness actuator, the so called Electro-Pneumatic Adaptable Impedance Actuator (EPAIA). EPAIA is designed to be applied, but not limited, to a rehabilitation robotics scenario. In order to guar-

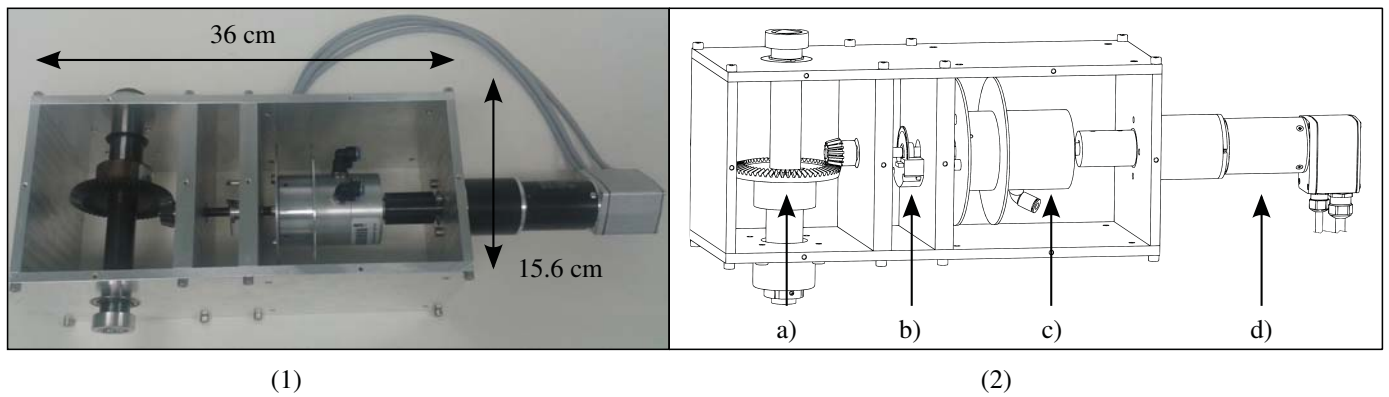


Fig. 1. EPAIA dimensions and components: (a) Bevel gear, (b) load encoder, (c) pneumatic spring, (d) Maxon motor EC45 with planetary gear and encoder.

ante the required supportive torque and reduce adverse effects, a stiff brushless DC-motor with gear box reduction is placed in series with a pneumatic rotational actuator, used as a continuously adaptable nonlinear pneumatic spring. The actuator comprises simple mechanical design, while at the same time a large stiffness range can be continuously adapted. Model equations for EPAIA are derived with the Lagrange-formalism and lead to a detailed nonlinear model. Based on this model, an optimal controller is designed for torque control. The controller is based on a convex optimisation procedure including an additional constraint to guarantee a positive-real controller and load impedance transfer function.

2. MECHANICAL DESIGN OF EPAIA

The electro-pneumatic actuator is shown in Fig. 1 and consists of a brushless direct current (BLDC)-motor with encoder and planetary gear box (d), an electronic power and control unit, a pneumatic torsional spring (c), a proportional valve, two pressure sensors, a second encoder (b), a bevel gear box (a) and a housing. In order to be used in movement assistance, the actuator has to guarantee a certain maximum torque and angular velocity, leading to a maximum (nominal) motor power. For our case, providing assistance to a knee joint, the maximum power is derived from kinematic data (Kong et al. (2012)). The data is obtained for a healthy person of 70 kg showing an average power of 70-80 W, needed for sufficient support. Including a safety margin of factor 2, covering transmission power reduction due to non-ideal mechanical elements, an electrical motor of 150 W is chosen (EC 45, Maxon Motor AG, Sachseln, Switzerland). On the one hand, the typical maximum angular velocity arising in normal walking is estimated with an upper bound of $|\omega_k| = 60$ rpm thus leading to an upper design bound for angular velocity of $|\omega_{k,max}| = 120$ rpm considering a safety factor of 2. On the other hand, the maximum torque is specified to be below $|M_{k,max}| \leq 40$ Nm. Using this information, gearbox reduction ratios have to be determined, where here two degrees of freedom are available. However, considering the natural operating range of stiffness values of the torsional pneumatic spring of 4.21 to 29.5 Nm/rad for operating pressures of 1 to 7 bar, a bevel gearbox reduction ratio of 4:1 was chosen to transform the stiffness of the spring at the joint (16.8 to 118 Nm/rad, for more details refer to Section 3). Note that this reduction ratio is an important parameter due to the mechanical realisation of relative torsional spring displacement at the knee joint rotation angle range. Fig. 2 shows the numerically predicted stiffness values for different initial chamber pressures.

Three exemplary curves at low medium and high chamber pre-tension show the possible range of stiffness values. Since the pneumatic pressure supply tubes of the rotational pneumatic spring are mechanically guided via the housing, sufficient space for uncoiling has to be provided for the knee rotation angle range times gear reduction ratio. Thus, to obtain the required torque, the planetary gearbox (GP 52, Maxon Motor AG, Sachseln, Switzerland) at the motor was selected with a reduction ratio of 26:1. The resulting maximum torque of the BLDC motor, disregarding any efficiency reduction of the gears, is 174 mNm. However, with a maximum stall torque of 1656 mNm the maximum load torque over a short period of time can be 667.5 mNm. The pneumatic torsional spring is chosen considering maximum torque, minimum constructed space and the resulting stiffness range, which depends on chamber pressure and volume. As a rotary pneumatic actuator, a relatively small actuator was selected (M/60284/TI, Norgen GmbH, Alpen, Germany), which is able to deliver 9.5 Nm at 6 bar chamber pressure. Table A.1 in Appendix A lists all important parameters for the pneumatic rotary spring. Since for a higher stiffness of the pneumatic spring a small chamber volume is of paramount importance, blocking valves were implemented in the first prototype (153467 HE-2-QS-6, Festo, Esslingen am

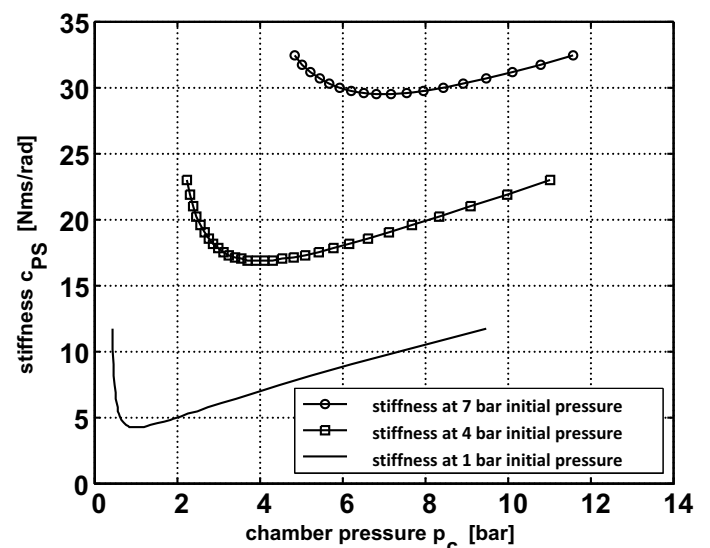


Fig. 2. Stiffness of the pneumatic torsional spring, evaluated at different initial chamber operating pressures and over pressure range.

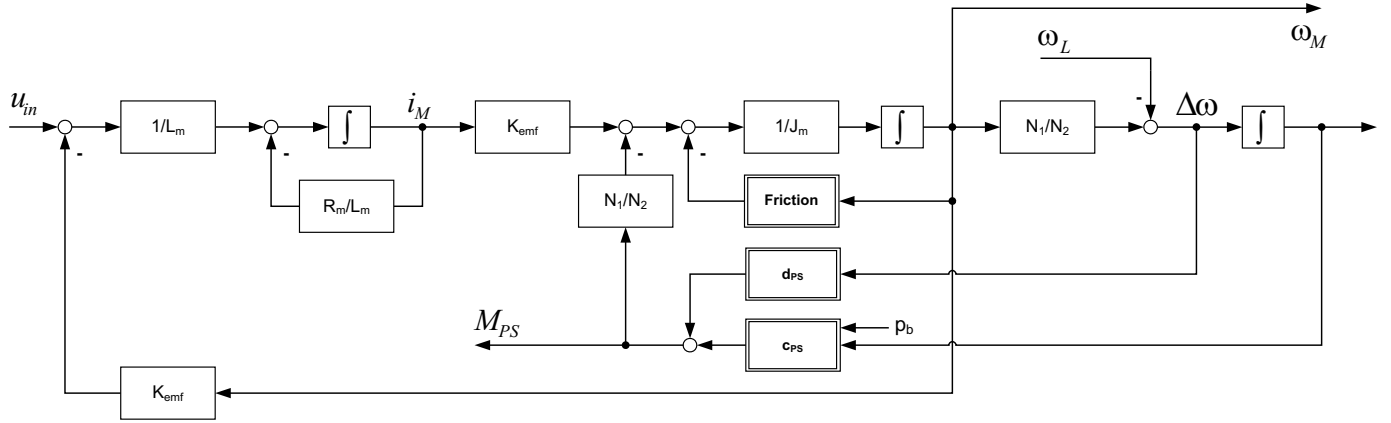


Fig. 3. System model of the brushless DC-motor with gearbox reduction and load coupling with input: $\mathbf{u} = [u_{in} \phi_L]^T$ and output: $\mathbf{y} = [\omega_M M_L]$.

Neckar, Germany). The coiling and uncoiling of the pressure supply tubes is guided by holding plates. The motor angle is measured using an encoder (HEDL 9140, Maxon Motor AG, Sachseln, Switzerland). A second encoder is included between pneumatic rotary spring and bevel gear reduction (AEAT-9000-1GSH1 including codewheel HEDG-9000-H13, Avago Technologies, San Jose, California, USA). Using both, encoder values and the pressure of the pressure chambers, measured by two pressure sensors (SDE5-D10, Festo, Esslingen am Neckar, Germany), the torque over the pneumatic rotary spring can be calculated. Finally, the bevel gear (40 15 1400, Atlanta, Bietigheim-Bissingen, Germany) is made from hardened steel and is designed to cover a maximum torque of up to 40 Nm. Important mechanical parameters of EPAIA are summarised in Table A.2 in Appendix A.

3. SYSTEM MODELLING

The actuator system is modelled by using the Lagrange formalism. Consider the Euler-Lagrange equations

$$\frac{d}{dt} \frac{\partial L}{\partial \dot{\mathbf{q}}_i} - \frac{\partial L}{\partial \mathbf{q}_i} = \tau_i = \frac{\partial W}{\partial \mathbf{q}_i}, \quad (1)$$

for which the number i of external forces is τ_i , the external work is W . The number of generalised coordinates q_i are expressed by the column vector

$$\mathbf{q}^T = [q_1 \ q_2 \ \dots \ q_i \ \dots \ q_M] \quad (2)$$

for the M degrees-of-freedom system. In (1), L is the Lagrange-function, which is a scalar function defined as the difference between kinetic $T(\mathbf{q}_i, \dot{\mathbf{q}}_i)$ and potential $V(\mathbf{q}_i)$ energy

$$L = T(\mathbf{q}_i, \dot{\mathbf{q}}_i) - V(\mathbf{q}_i). \quad (3)$$

In the following section, the Lagrange-function is set-up for each subsystem, with a subsequent derivation of the Euler-Lagrange equations. For the sake of clarity and to avoid confusion with electrical charge, we will use the original physical variables instead of \mathbf{q} .

Generalised coordinates for the electrical motor are the electrical charge q_M and the angle of the mechanical shaft ϕ_M (with derivatives I_M and ω_M , respectively). The kinetic energy of the system consists of energy, stored in the armature coil and the rotation of the mechanical shaft

$$T = \frac{J_M}{2} \omega_M^2 + \frac{L}{2} I_M^2 \quad (4)$$

with J_M the rotor inertia, L the armature inductivity, ω_M the revolution speed and I_M the BLDC-motor current.

The potential energy of the system consists of energy, stored in the pneumatic spring

$$V = \frac{c_{PS}(\phi, p_b)}{2} \phi^2 \quad (5)$$

with c_{PS} the stiffness of the spring, p_b is the basic chamber pressure and ϕ the angle of deflection. The external forces acting on the electrical system can be stated as

$$\partial W_e = U_M \partial q_M - R \dot{q}_M \partial q_M - K_{M,emf} \dot{\phi}_M \partial q_M, \quad (6)$$

in which U_M is the external motor supply voltage, R is the armature resistance, q_M is electrical charge and $K_{M,emf}$ is the back-electromotive force (EMF). The external forces acting on the mechanical system are given by

$$\begin{aligned} \partial W_m = & -M_{R1} \dot{\phi}_M \partial \phi_M - \frac{N_1}{N_2} d_{PS}(\dot{\phi}) \left(\frac{N_1}{N_2} \dot{\phi}_M - \dot{\phi}_L \right) \partial \phi_M \\ & + K_{M,emf} I_M \partial \phi_M, \end{aligned} \quad (7)$$

with M_{R1} the rotor viscous friction, $\phi = \frac{N_1}{N_2} \phi_M - \phi_L$ is the spring deflection angle, ϕ_L is the load angle, d_{PS} is the damping of the spring and M_{PS} the moment over the pneumatic spring. The differential equations for the BLDC-motor follow as

$$\begin{aligned} \frac{d}{dt} I_M = & -\frac{R}{L} I_M - \frac{K_{M,emf}}{L} \omega_M + \frac{1}{L} U_M \\ \frac{d}{dt} \omega_M = & \frac{K_{M,emf}}{J_M} I_M - \left[\frac{M_{R1}(\omega_M)}{J_M} + \left(\frac{N_1}{N_2} \right)^2 \frac{d_{PS}(\dot{\phi})}{J_M} \right] \omega_M \\ & - \frac{N_1}{N_2} \frac{c_{PS}(\phi, p_b)}{J_M} \phi - \frac{N_1}{N_2} \frac{d_{PS}(\dot{\phi})}{J_M} \omega_L \\ \frac{d}{dt} \phi = & \frac{N_1}{N_2} \omega_M - \omega_L \end{aligned} \quad (8)$$

in which $M_{R1}(\omega_M)$ is nonlinear friction and $c(\phi, p_b)$ is the stiffness of the torsional pneumatic spring. We assume an isothermal process for the torsional pneumatic spring with $p_{a,1} V_{a,1} = p_{a,2} V_{a,2}$, denoting the system change under constant temperature. The moment acting on pneumatic impeller is given by

$$M(p_c) = \int_{r_1}^{r_2} p_c l_i r dr \quad (9)$$

$$= p_c l_i \frac{1}{2} (r_2^2 - r_1^2) = p_c k_{volume}, \quad (10)$$

where p_c is the pressure of a single chamber, l_i is the length of the pneumatic impeller, and r_1 and r_2 are the start and end of the impeller, as seen from torsional pneumatic spring centre, respectively. The volume of the chamber V_c decreases or increases with the impeller deflection ϕ as

$$V_t = V_c \frac{\theta_B \pm \phi}{\theta_B} + V_{tub}, \quad (11)$$

in which V_t denotes the total volume and θ_B denotes the maximum deflection angle. Combining equations (10) and (11) leads to the following equation

$$M_c(\phi, p_c) = p_b \frac{V_c + V_{tub}}{V_c \frac{\theta_B \pm \phi}{\theta_B} + V_{tub}} k_{volume}. \quad (12)$$

The moment thus depends on the basic chamber pressure p_b and an angle deflection ϕ . The torsional pneumatic spring consists of four chambers of which two in each case are connected and two are arranged such, that they are opposing each other. On a nonzero deflection angle, the air in the two chambers is compressed while at the same time an expansion of the air in the other two chambers takes place. The following expression for the moment is obtained

$$\begin{aligned} M_{PS}(\phi, p_b) &= 2M_{c1} - 2M_{c2} \\ &= 2p_b(V_c + V_{tub})k_{volume} \frac{-2\theta_B V_c}{V_c^2 \phi^2 - \theta_B^2(V_c + V_{tub})^2} \phi, \end{aligned} \quad (13)$$

and the stiffness of the spring

$$c_{PS}(\phi, p_b) = 4p_b(V_c + V_{tub})k_{volume} \frac{-\theta_B V_c}{V_c^2 \phi^2 - \theta_B^2(V_c + V_{tub})^2}. \quad (14)$$

The friction in the motor and damping term of pneumatic spring can be modelled by

$$M_{R1}(\omega_M) = M_{fM0} * \text{sign}(\omega_M) + M_{fM1} * \omega_M \quad (15)$$

and

$$d_{PS}(\Delta\omega) = M_{fPS0} * \text{sign}(\Delta\omega) + M_{fPS1} * \Delta\omega. \quad (16)$$

Defining the model outputs as $\mathbf{y}^T = [I_M \ \omega_M \ M_{PS}]$, inputs $\mathbf{u}^T = [U_M \ \omega_L]$ and states $\mathbf{x}^T = [I_M \ \omega_M \ \phi]$, the linear state-space equations are obtained by using standard Taylor-approximation, neglecting higher terms than order one

$$\begin{aligned} \mathbf{A} &= \begin{bmatrix} -\frac{R}{L} & -\frac{K_{emf}}{L} & 0 \\ \frac{K_{emf}}{J_M} & -\frac{1}{J_M} \left[\frac{\partial M_{R1}}{\partial \omega_M} + \frac{N_1^2 \partial d_{PS}(\cdot)}{N_2^2 \partial \omega_L} \right] & -\frac{N_1}{N_2 J_M} \frac{\partial c_{PS}(\cdot)}{\partial \phi} \\ 0 & \frac{N_1}{N_2} & 0 \end{bmatrix} \\ \mathbf{B} &= \begin{bmatrix} \frac{1}{L} & 0 & 0 \\ 0 & -\frac{N_1}{N_2} \frac{1}{J_M} \frac{\partial d_{PS}(\cdot)}{\partial \omega_M} & -1 \end{bmatrix}^T, \\ \mathbf{C} &= \begin{bmatrix} 1 & 0 & 0 \\ 0 & 1 & 0 \\ 0 & \frac{N_1}{N_2} \frac{\partial d_{PS}(\cdot)}{\partial \omega_M} & \frac{\partial c_{PS}(\cdot)}{\partial \phi} \end{bmatrix} \\ \mathbf{D} &= \begin{bmatrix} 0 & 0 & 0 \\ 0 & 0 & -\frac{\partial d_{PS}(\cdot)}{\partial \omega_L} \end{bmatrix}^T \end{aligned} \quad (17)$$

4. CONTROLLER DESIGN

As the first step of the design procedure, a motor current controller is designed using the linear quadratic regulator approach, minimising the cost function

$$J(u) = \int_0^\infty (\mathbf{x}^T \mathbf{Q} \mathbf{x} + u_{in} R u_{in}) dt, \quad (18)$$

with respect to the linearised plant (17) and with weightings $\mathbf{Q} = \mathbf{Q}^T \geq 0$, defined here as diagonal state-weighting matrix $\mathbf{Q} = \text{diag}(q_1, q_2, 0, 0)$ and the control input weighting $R \in \mathbb{R}_+$. The current controlled state space model, represented by matrices $(\mathbf{A}_1, \mathbf{B}, \mathbf{C}, \mathbf{D})$, is subsequently brought to transfer function matrix representation $\mathbf{G}(s) = \mathbf{C}(s\mathbf{I} - \mathbf{A}_1)^{-1}\mathbf{B} + \mathbf{D}$. High frequency dynamics of the transfer function

$$\mathbf{G}(s) = \frac{1}{(s + \alpha_1)(s^2 + \alpha_2 s + \alpha_3)} \begin{bmatrix} \beta_{11}s & \beta_{12}(s + \alpha_1)(s + \alpha_4) \\ \beta_{21} & \beta_{22}(s + \alpha_1)(s + \alpha_4)(s + \gamma) \end{bmatrix}, \quad (19)$$

corresponding to the pole of the current dynamics $p_1 = -\alpha_1 = 5.723 \cdot 10^3$ rad/s are neglected. In (19), system parameters α_2, α_3 , and $\beta_{11}, \beta_{12}, \beta_{21}, \beta_{22}$ are obtained from state-space conversion and have to be corrected for the numerator constants to $\bar{\beta}_{11} = \frac{\beta_{11}}{\alpha_1}$ and $\bar{\beta}_{21} = \frac{\beta_{21}}{\alpha_1}$. The system of reduced order and input dimension $\mathbf{G}_{red,1}(s) : u_{in,1}(s) \mapsto [\omega_m(s) M_{PS}(s)]^T$ is given by

$$\mathbf{G}_{red,1}(s) = \frac{1}{s^2 + \alpha_2 s + \alpha_3} \begin{bmatrix} \bar{\beta}_{11}s \\ \bar{\beta}_{21} \end{bmatrix}, \quad (20)$$

where $u_{in,1}$ is the new control input variable of the current controlled system. We propose a post-compensator for (20), which is based on the idea to place the compensator induced transmission zero such, that the phase of the plant near crossover frequency is increased, obtaining a squared down system.

Let the Smith and the Smith-McMillan form for the system (20) be given by

$$\mathbf{U}(s)\mathbf{S}(s)\mathbf{V}(s) = \begin{bmatrix} \bar{\beta}_{11}s \\ \bar{\beta}_{21} \\ 1 \\ 0 \end{bmatrix} \begin{bmatrix} 1 \\ 0 \end{bmatrix} \bar{\beta}_{21} = \begin{bmatrix} \bar{\beta}_{11}s \\ \bar{\beta}_{21} \end{bmatrix}. \quad (21)$$

We define post-compensator by introducing the row vector $\mathbf{C}_c(s) = [a \ 1]$, in which a is a proportional-gain applied to the motor speed and the property of the open-loop torque function over the pneumatic spring M_{PS} should not be changed by $\mathbf{C}_c(s)$ in the low frequency range. By using (21), the set of transmission zeroes can be obtained by solving

$$\det \left(\mathbf{C}_c(s) \cdot \begin{bmatrix} \bar{\beta}_{11}s \\ \bar{\beta}_{21} \\ 1 \end{bmatrix} \right),$$

for which we obtain

$$z_t = -\frac{\bar{\beta}_{21}}{\bar{\beta}_{11}} \cdot \frac{1}{a}.$$

The transmission zero is placed such that phase and bandwidth of the open-loop squared down system are increased for torque interaction control. Towards this goal, we choose a zero position $z_t = 1.5918\omega_{c,PS}$, with $\omega_{c,PS}$ the crossover frequency of the open-loop transfer function from $u_{in,1}(s)$ to $M_{PS}(s)$. The post-compensator parameter results in $a = 0.038\text{Hz}$, which leads to an increase of 10.5 deg. in phase and 0.5 dB in magnitude at the crossover frequency $\omega_{c,PS}$.

The reduced-order squared down plant $\mathbf{G}_{red}(s)\mathbf{C}_c(s)$ is subsequently extended by weighting functions to shape sensitivity

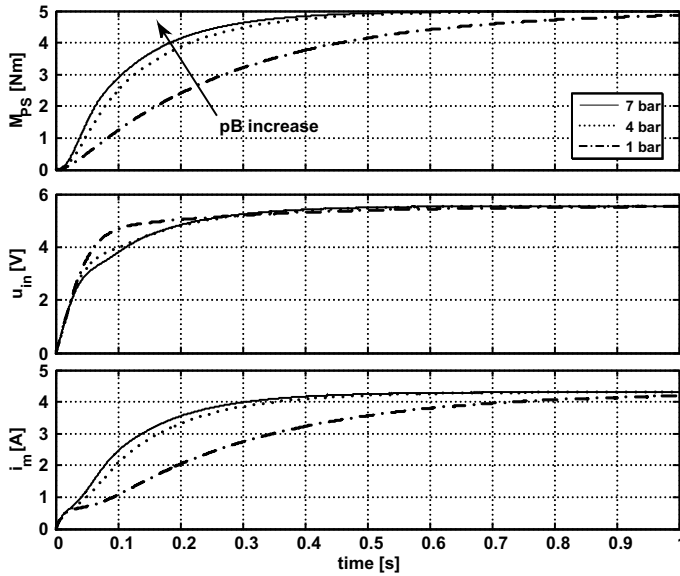


Fig. 5. Closed-loop system response to a reference step of 5 Nm magnitude at fixed load conditions and at varying chamber pre-pressure, of 1,4 and 7 bar.

$\mathbf{K} = \mathbf{L}_2^T \mathbf{W}^{-1} + \tilde{\mathbf{D}}_{12}^T \tilde{\mathbf{C}}_1$ (for the proof under orthogonal plant assumptions refer to Geromel and Gapski (1997)) define the matrix decision variable $\mathbf{Z} = \mathbf{Z} \in \mathbb{R}^{q \times q}$ for which the minimization of the performance index

$$J = \min \text{tr}(\mathbf{Z})$$

for the system of LMI's

$$\begin{bmatrix} \mathbf{W} & (\tilde{\mathbf{C}}_1 \mathbf{W} - \tilde{\mathbf{D}}_{12} \mathbf{L}_2^T)^T \\ \tilde{\mathbf{C}}_1 \mathbf{W} - \tilde{\mathbf{D}}_{12} \mathbf{L}_2^T & \mathbf{Z} \end{bmatrix} \geq 0 \quad (33)$$

$$\tilde{\mathbf{A}} \mathbf{W} + \mathbf{W} \tilde{\mathbf{A}}^T - \mathbf{Q}_2 - \mathbf{L}_2 (\tilde{\mathbf{D}}_{21} \tilde{\mathbf{D}}_{21}^T) \mathbf{L}_2^T \leq 0.$$

associated with the state-feedback algebraic Riccati equation and (32) solves the problem (28). The gain matrix $\mathbf{K} = \mathbf{L}_2^T \mathbf{W}^{-1} + \tilde{\mathbf{D}}_{12}^T \tilde{\mathbf{C}}_1$ is successfully obtained, if (32) and (33) have a solution in \mathbf{W} and \mathbf{Z} . The obtained SPR-controller $\tilde{\mathbf{C}}_K(s)$ is transformed to the coordinate system of the generalised plant using

$$\mathbf{C}_K(s) = \mathbf{S}_y^{-1} \tilde{\mathbf{C}}_K(s) \mathbf{S}_u^{-1}. \quad (34)$$

Using the convex optimisation toolbox Yalmip (Lofberg (2004)), an 8th-order controller was calculated that successfully minimises the load impedance transfer function $Z(s)$ and guarantees $Z(s)$ to be positive-real.

5. RESULTS

The continuous time controller was discretised at $T_s = 0.0025$ s and implemented with a high-gain anti-windup feedback strategy (Hyde (1995)) to prevent excessive overshoot in cases of system input current limitation. Nonlinear model and controller were implemented in MATLAB/Simulink. For measurements at different pneumatic torsional spring stiffness values, both chambers of the pneumatic spring were initialised at chamber pressures, ranging from 1 to 7 bar. A number of tests for reference tracking, disturbance rejection and load impedance measurements were conducted with the closed-loop impedance controller and at varying load conditions. Fig. 5 shows the worst-case example of a step response at fixed load and with

varying pneumatic chamber pre-pressures of 1, 4 and 7 bar. As a reference value a unit step was applied to the impedance controller, corresponding in commanded input voltage and motor current. It can be easily seen that although the motor current is not in saturation and the system response is sufficiently fast for active knee support, with a rise time $t_{r,90}$ of 0.25s for the stiff pre-setting. The controller was tested in extensive simulations and over varying operating points of varying amplitude. Similar results like those shown in Fig. 5 were obtained in step like reference setpoint changes with larger torque amplitude, resulting in a nonlinear spring characteristic. However, note that varying the varying spring constant was not explicitly addressed in the controller design.

In addition to extensive reference tracking and disturbance rejection tests, the load impedance function $Z(s) = \frac{M_{PS}(s)}{\omega_L(s)}$ was analysed in closed-loop condition using the nonlinear plant. Fig. 6 shows the bode plot of the linearised feedback-controlled system. The range of possible load impedance variation for different pneumatic spring constants is given in Fig. 6. In addition, the positive-real property of $Z(s)$ is satisfied for all possible pneumatic spring stiffness values.

6. DISCUSSION AND OUTLOOK

In this contribution, the modelling and the design of an impedance controller was proposed for the novel type of an electro-pneumatic adaptable impedance actuator EPAIA. Using a detailed linearised version of a nonlinear model, obtained by the Lagrange formalism, a norm optimal \mathcal{H}_2 -controller was proposed to include an additional constraint leading to a strictly positive real controller design. The controller design procedure was rearranged to be better suited for loop-shaping approaches leading to a convex optimisation problem and was applied to the generalised plant, transformed by a similarity transformation to relax orthogonality assumptions. The controller design procedure included a squaring down approach with a resulting

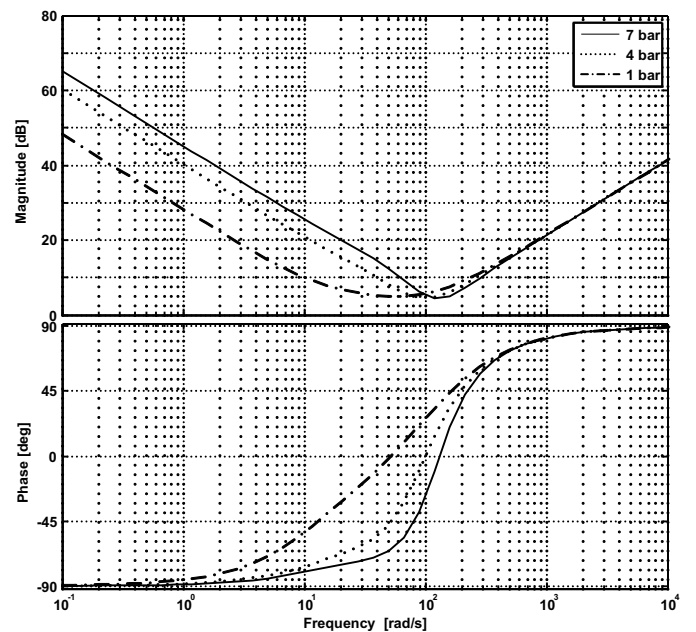


Fig. 6. Load impedance $Z(j\omega) = \frac{M_L(j\omega)}{\omega_L(j\omega)}$ frequency response with closed impedance control-loop and at different chamber pre-pressures.

quadratic system and the placement of a transmission zero. Furthermore, the minimisation of the load impedance function was taken into the controller design, maintaining the convex nature of the optimisation problem. The new control strategy showed good results in reference tracking when applied to the nonlinear time-varying system. EPAIA was able to provide the necessary torque and bandwidth required for exoskeleton-based knee support. Sufficient control of the nonlinear system with time-varying pneumatic spring stiffness was achieved by using only a single controller. However, adapting the controller gains, depending on the time-varying pneumatic spring is suggested to improve controller performance and load impedance transfer function. In addition to that, an online adaptation of the torsional pneumatic spring stiffness would result in a multivariable loop, since process coupling in the pneumatic rotational spring is introduced by controlling the pressure of the chambers. These issues are the subject of ongoing work.

Appendix A. MODEL AND DESIGN PARAMETERS

Table A.1. Parameters of the pneumatic torsional spring.

Description	Param.	Value	Unit
Diameter + tubes & sensors	D_{PS}	104.0	[mm]
Spring constant	c_{PS}	4.21 to 29.5	[Nm/rad]
Spring friction	d_{PS}	0.9	[Nms/rad]

Table A.2. Mechanical parameters of EPAIA.

Param.	Value	Unit	Param.	Value	Unit
R	1.29	[Ω]	L	$3.95 \cdot 10^{-4}$	[H]
K_{emf}	$44.5 \cdot 10^{-3}$	[V/rad/s]	I_{max}	15	[A]
J_M	119	[gcm^2]	U_N	48	[V]
N_1	1	[-]	N_2	26	[-]
V_c	$17 \cdot 10^{-6}$	[m^3]	k_{volume}	$3.8 \cdot 10^{-5}$	[m^3]
α_1	$5.72 \cdot 10^3$	[-]	α_2	79.97	[-]
α_3	7.87	[-]	β_{11}	$9.47 \cdot 10^6$	[-]
β_{12}	$3.64 \cdot 10^4$	[-]	β_{21}	323.21	[-]
β_{22}	-0.1	[-]	β_{11}	$1.65 \cdot 10^3$	[-]
β_{12}	6.36	[-]	γ	75.25	[-]
α_4	50	[-]			

Table A.3. CONTROLLER WEIGHTINGS AND PARAMETERS.

Param.	Value	Unit	Param.	Value	Unit
k_2	0.1	-	z_2	1.25	-
p_2	$1.25 \cdot 10^{-2}$	-	k_{11}	1000	-
z_{11}	$2.94 \cdot 10^{-2}$	-	p_{11}	$2.94 \cdot 10^2$	-
z_{12}	$9.55 \cdot 10^{-2}$	-	p_{12}	$1.11 \cdot 10^{-2}$	-
$p_{12,HF}$	$1 \cdot 10^{-3}$	-			

REFERENCES

Cavagna, G., Heglund, N., and Taylor, C. (1977). Mechanical work in terrestrial locomotion: Two basic mechanism for minimizing energy expenditure. *Am. J. Physiology*, 233 – 261.

Geromel, J. and Gapski, P. (1997). Synthesis of positive real \mathcal{H}_2 controllers. *Automatic Control, IEEE Transactions on*, 42(7), 988–992.

Grebenstein, M., Albu-Schaeffer, A., Bahls, T., Chalon, M., Eiberger, O., Friedl, W., Gruber, R., Haddadin, S., Hagn, U., Haslinger, R., Hoppner, H., Jorg, S., Nickl, M., Nothhelfer,

Table A.4. Components of the EPAIA (Abbreviations: M. for motor, E. for encoder, P. for pneumatic, res. for resolution)

Component	Type and manufacturer	Remarks
Motor	150 Watt BLDC-Motor EC 45, (Maxon Motor AG, Switzerland)	$M_{nom} = 174$ mNm
Gear	Planetary gear 52, (Maxon Motor AG, Switzerland)	$N_1/N_2 = 26$
M. E.	Encoder HEDL 9140, (Maxon Motor AG, Switzerland)	500 lines/rev.
M. controller	ESCON Modul 50/5, (Maxon Motor AG, Switzerland)	I_M cont. mode
P. spring	M/60284/TI/90 (Norgren GmbH, Germany)	$c_{PS,max} = 120 \frac{Nm}{rad}$
Load E.	AEAT-9000-1GHS1 (Avago Technologies, USA)	optical, 17 bit res.
Bevel gear	40 15 400 spur-toothed (Atlanta, Germany)	$N_1/N_2 = 4$
p sensor	SDES-D10 (Festo, Germany)	range 1...11 bar

A., Petit, F., Reill, J., Seitz, N., Wimbock, T., Wolf, S., Wusthoff, T., and Hirzinger, G. (2011). The DLR hand arm system. In *Robotics and Automation (ICRA), 2011 IEEE International Conference on*, 3175–3182.

Ham, R., Sugar, T., Vanderborght, B., Hollander, K., and Lefeber, D. (2009). Compliant actuator designs. *Robotics Automation Magazine, IEEE*, 16(3), 81–94.

Hogan, N. (1984). Adaptive control of mechanical impedance by coactivation of antagonist muscles. *Automatic Control, IEEE Transactions on*, 29(8), 681 – 690.

Hyde, R. (1995). *\mathcal{H}_∞ aerospace control design: a VSTOL flight application*. Advances in industrial control. Springer.

Kong, K., Bae, J., and Tomizuka, M. (2012). A compact rotary series elastic actuator for human assistive systems. *Mechatronics, IEEE/ASME Transactions on*, 17(2), 288–297.

Lofberg, J. (2004). Yalmip: a toolbox for modeling and optimization in matlab. In *IEEE International Symposium on Computer Aided Control Systems Design*, 284–289.

Misgeld, B., Gerlach-Hahn, K., and Leonhardt, S. (2012). Biomimetic actuator control for a pneumatic cylinder. In *IFAC Symposium on Biological and Medical Systems*, 218–223.

Pratt, G. and Williamson, M. (1995). Series elastic actuators. In *Proceedings of the IEEE/RSJ International Conference on Intelligent Robots and Systems*, 399 – 406.

Pratt, G.A., Williamson, M.M., Dillworth, P., Pratt, J., Ull, K., and Wright, A. (1995). Stiffness isn't everything. In *Proceedings of ISER*, 253–262.

Vallery, H., Ekkelenkamp, R., van der Kooij, H., and Buss, M. (2007). Passive and accurate torque control of series elastic actuators. In *Intelligent Robots and Systems, 2007. IROS 2007. IEEE/RSJ International Conference on*, 3534–3538.

Zinn, M., Khatib, O., Roth, B., and Salisbury, J. (2003). Actuation methods for human-centered robotics and associated control challenges. In *Springer Tracts in Advanced Robotics*, 105 – 119.